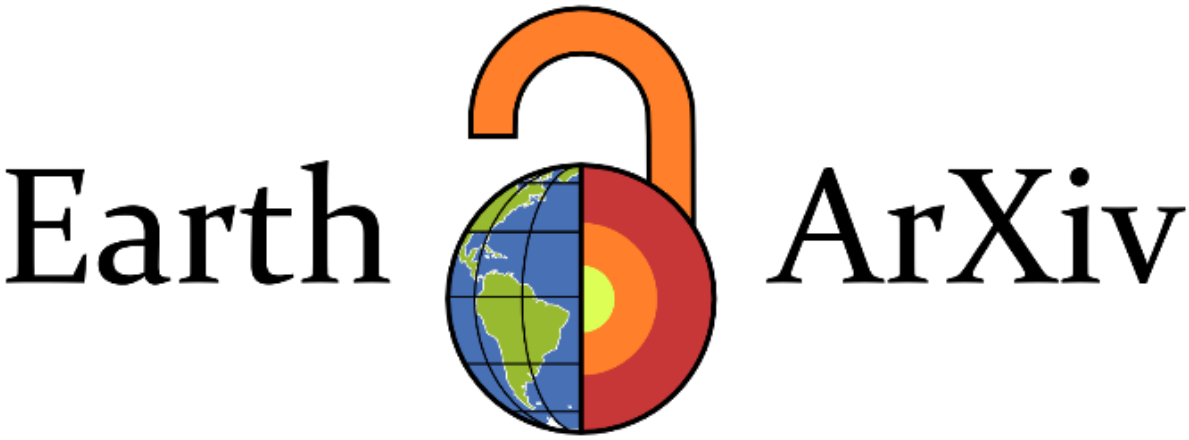

Large earthquakes are more predictable than smaller ones

Patricio Venegas-Aravena[1,*] and Davide Zaccagnino[2,3,**]

1. Department of Structural and Geotechnical Engineering, School of Engineering, Pontifical Catholic University of Chile, Vicuña Mackenna 4860, Macul, Santiago, Chile

2. Earth Sciences Department, Sapienza University, Piazzale Aldo Moro, 5, 00185, Rome, Italy.

3. National Institute of Geophysics and Volcanology (INGV), Via di Vigna Murata, 605, 00143, Rome, Italy.

* plvenegas@uc.cl

** davide.zaccagnino@uniroma1.it

Orcid:

P.V.-A.: https://orcid.org/0000-0003-3777-0941

D.Z.: https://orcid.org/0000-0001-6884-8452

Author contributions statement

P.V-A.: Conceptualization, Formal analysis, Investigation, Methodology, Project Administration, Software, Resources, Supervision, Validation, Visualization, Writing – original draft and review & editing; D.Z.: Conceptualization, Data Curation, Formal analysis, Funding Acquisition, Investigation, Methodology, Software, Validation, Visualization, Writing – original draft and review & editing.

Abstract

Large earthquakes have been viewed as highly chaotic events regardless of their magnitude, making their prediction intrinsically challenging. Here, we develop a mathematical tool to incorporate multiscale physics, capable of describing both deterministic and chaotic systems, to model earthquake rupture. Our findings suggest that the chaotic behavior of seismic dynamics, that is, its sensitivity to initial and boundary conditions, is inversely related to its magnitude. To validate this hypothesis, we performed numerical simulations with heterogeneous fault conditions. Our results indicate that large earthquakes, usually occurring in regions with higher residual energy and lower b-value (i.e., the exponent of the Gutenberg-Richter law), are less susceptible to perturbations. This suggests that a higher variability in earthquake magnitudes (larger b-values) may be indicative of structural complexity of the fault network and heterogeneous stress conditions. To further validate our findings, we compare our theoretical predictions with real seismicity in Southern California; specifically, the relationship between the b-value and the fractal dimension of hypocenters with our model predictions finding good agreement. The statistical similarities observed between the simulated and real earthquakes support the hypothesis that large earthquakes may be less chaotic than smaller ones; hence, more predictable.

Keywords: Earthquake predictability; Seismic rupture; Chaos theory; Residual energy; b-value; HE-B method.

1. Introduction

Earthquakes are a persistent threat to human society, capable of causing widespread devastation (e.g., Kahandawa et al., 2018). The rapid release of accumulated tectonic stress can result in catastrophic natural disasters with severe human and economic consequences (Knopoff, 1958; Vassiliou and Kanamori, 1982; Gudmundsson, 2014; Aksoy et al., 2024; Silverio-Murillo et al., 2024). To efficiently face seismic risk, a deeper understanding of seismicity is needed. Particularly, a fundamental aspect of earthquake studies is the examination of rupture processes along geological faults (e.g., Christensen and Beck, 1994; Kintner et al., 2018; Otarola et al., 2021; Martínez-Lopez, 2023; Wang et al., 2023), as these can induce notable changes in the soil's physical characteristics, such as variations in ground velocity, acceleration and frequency (Colavitti et al., 2022; Li et al., 2022; Venegas-Aravena, 2024). Evidence from various studies points to the possibility that seismic rupture processes may exhibit the hallmarks of chaotic systems, suggesting a complex and unpredictable nature of these events. Some perspectives on earthquake generation are rooted in simplified spring-block models which exhibit these chaotic dynamics (e.g., Huang and Turcotte, 1990; Gualandi et al., 2023). This is reflected in computational simulations where small variations in the initial conditions generate completely different rupturing scenarios (e.g., Erickson et al., 2011). That is, causing no correlation between a priori and a posteriori parameter (Venegas-Aravena et al., 2024). Despite this complexity, a consistent finding from these simulations is the emergence of a single dominant parameter: residual energy. The importance of the accumulated/residual strain is also coherent with recent results in the modeling of paleoseismic recordings (Salditch et al., 2020). This parameter,

which defines zones where ruptures are prone to occur (Noda et al., 2022), appears to exert a controlling influence on both the spatial extent and temporal evolution of ruptures (Venegas-Aravena, 2023; Venegas-Aravena et al., 2024). Its value is dependent on both the available energy, which is determined by the initial stresses, and the fracture energy, which is associated with the energy required to continue propagating the rupture (Noda et al., 2022). Therefore, when the rupture front approaches a zone with negative (positive) stress release rate, more (less) energy is consumed in generating the rupture, causing the rupture to arrest (continue propagating). Other formalisms associated with friction have also found that rupture arrest can be related to stresses and fracture energy (Barras et al., 2023).

Residual energy has been linked to a parameter called thermodynamic fractal dimension D (Venegas-Aravena and Cordaro, 2023a). This quantity is useful for characterizing fault distribution (Zou and Fialko, 2024) and the spatial distribution of global seismicity (Perinelli et al., 2024). For instance, it has been observed that the fractal dimension decreases prior to a major earthquake, suggesting a transition from a more diffuse, three-dimensional seismicity distribution to a more localized, planar distribution along the fault (Murase, 2004; Wyss et al., 2004; Iaccarino and Picozzi, 2023). Other studies have interpreted this decrease in D as an indicator of an impending larger rupture due to the increase of shear stresses (e.g., Ito and Kaneko, 2023; Venegas-Aravena and Cordaro, 2023a). Furthermore, it has been linked to the b-value, a parameter describing earthquake frequency (Venegas-Aravena and Cordaro, 2023b). Given the proportional relationship between D and the b-value, a decrease in D is also associated with a decrease in the b-value prior to large earthquakes.

Given the link between the parameter D and properties associated with chaotic systems, as suggested by lower D values in less chaotic systems (Venegas-Aravena and Cordaro 2024), the b-value is anticipated to provide insights into the chaotic states of faults. To explore this connection, Section 2 delves into the fundamental principles of multiscale thermodynamics applied to faults. Section 3 presents various simulations of heterogeneous ruptures, facilitating the interpretation of parameters such as D and the b-value within the framework of multiscale thermodynamics and chaotic systems. In Section 4, we apply these concepts to a real fault system, specifically in Southern California, to support our theoretical and numerical results. A discussion and conclusion are presented in Sections 5 and 6 respectively.

2. Theoretical background: multiscale thermodynamics

As earthquakes are essentially multi-scale events that may exhibit chaotic behavior, a physical framework is required to fully understand their dynamics. In this regard, Venegas-Aravena and Cordaro (2024) have developed a quantitative relationship linking the sum of the Lyapunov exponents Λ, to the thermodynamic fractal dimension D, expressed as:

$$\Lambda \sim e^{\frac{(D_E - D - 1)}{k_V}} \tag{1}$$

The Euclidean dimension is denoted by D_E, while k_V is a constant associated with the system's scale. D is a parameter that characterizes the distribution of systems exhibiting power-law behavior. For simplicity, k_V is assigned a value of 1. This relationship can be observed in Figure 1a, where low (large) values of Λ are

120 associated with low (large) values of D. A higher value of Λ indicates that the
121 system is more susceptible to the influence of small changes in initial conditions
122 (Ruelle, 1983; Tabor, 1989), whereas a more negative value of Λ suggests that
123 the system is less sensitive to these initial conditions, which could be considered
124 as being more regular. The sign of Λ provides an indication of whether a system
125 is non-reversible/dissipative (negative sum) or conservative (e.g., Hoover and
126 Posch, 1994). Given that the brittle crust is a system characterized by the
127 dissipation of stored energy, the sum of Λ is a more relevant metric than the
128 largest Lyapunov exponent, often used to determine the chaotic nature of a
129 system. Consequently, lower values of D correspond to less chaotic systems, i.e.,
130 less sensitive to initial conditions. In the case of earthquakes, D can be related to
131 the magnitude of seismic events through the equation (Venegas-Aravena and
132 Cordaro 2023a):

133 $$M_W \sim \log_{10} e^{-\alpha(D)} \qquad (2)$$

134 Where $\alpha(D) = pD/k_V$ and $p = 3/(5 - D)$. From Equation 1, D can be written in
135 terms of the sum of the Lyapunov exponent as $D = (D_E - 1) - k_V \ln \Lambda$. By
136 substituting this Equation into Equation 2, we can establish a direct relationship
137 between the magnitude and chaotic systems as:

138 $$M_W = M_W(\Lambda) \qquad (3)$$

139 This relationship is graphically depicted in the color-coded maps presented in
140 Figures 1a, 1b, and 1c. In these maps, red tones correspond to earthquakes of
141 greater magnitude, while blue tones represent smaller earthquakes. Notably, in
142 Figure 1a, large earthquakes are correlated with lower values of both D and λ.
143 This finding implies that larger seismic events exhibit a reduced sensitivity to

initial conditions. In contrast, smaller earthquakes (represented by blue hues in Figure 1a) are associated with a higher degree of chaos, suggesting that these events originate in a more chaotic environment where even small perturbations can lead to seismic activity of varying scales, from small to intermediate.

This phenomenon is coherent with several observations suggesting the strong sensitivity of small seismicity to stress perturbations, e.g., tides and hydrological modulations (Rubinstein et al., 2008; Petrelis et al., 2021), which are not reported for major events (Vidale et al., 1998; Kossobokov and Panza, 2020). To delve deeper into this phenomenon, it is imperative to examine the energy conditions within the fault, specifically the concept of residual energy, E^{res} (Noda et al., 2021). This energy parameter serves as a criterion for the initiation of ruptures, indicating that a positive E^{res} value signifies a greater propensity for a fault to generate ruptures, while negative values diminish this likelihood. Mathematically, this energy can be expressed as:

$$E^{res} = \Delta W_0 - G_C \tag{4}$$

Where ΔW_0 represents the available energy, which can be correlated with the elastic energy stored within the system, and G_C denotes the fracture energy, characterizing the resistance to rupture propagation. This equation can be expressed in terms of D as follows:

$$E^{res} \sim e^{-\frac{D}{2k_V}} - d_0 10^D \tag{5}$$

Where d_0 is constant. Figure 1b illustrates the relationship between E^{res}, Λ, and earthquake magnitude (color-coded map). Higher E^{res} values correlate with lower Λ values, suggesting that regions more prone to rupture are also less sensitive to

initial conditions. Given that these regions are associated with large earthquakes (red colors), it is proposed that areas with high residual energy have higher chances to host a major event as a response to stress perturbations.

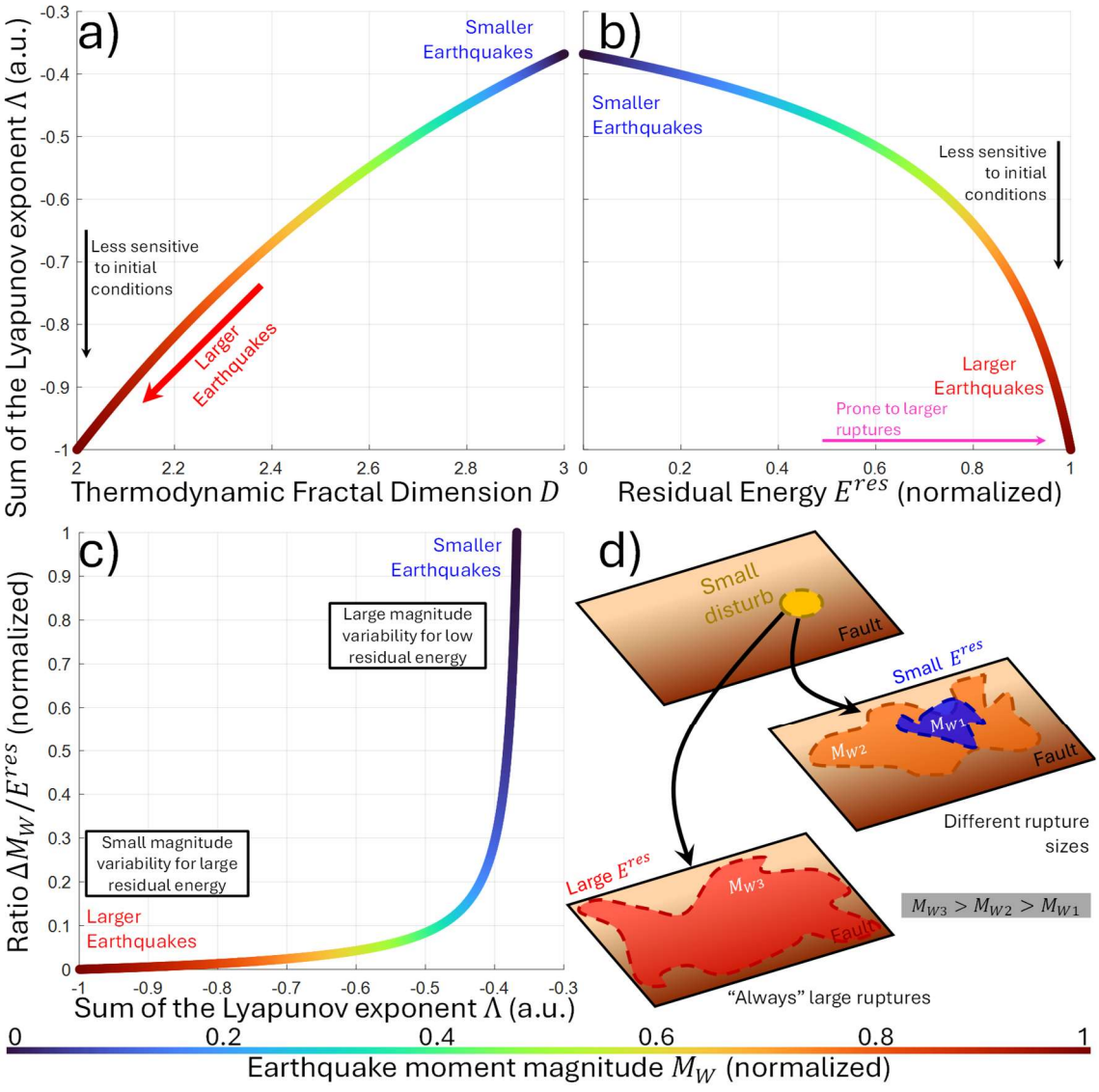

Figure 1: a) Equation 1 reveals a relationship between the sum of Lyapunov exponents Λ and the thermodynamic fractal dimension D. Systems with low sensitivity to initial conditions (highly negative Λ values) correspond to low D values. Colors indicate event magnitudes as calculated by Equation 2. Large events (red hues) are associated with low D and low Λ. b) Equation 5

relates Λ to residual energy (E^{res}). Higher E^{res} values correlate with a higher probability of large earthquakes, which in turn are linked to lower chaos and larger events. c) The plot of magnitude changes for a given E^{res} versus Λ shows that small (large) earthquakes exhibit greater (lesser) magnitude variability for low (high) E^{res}, as indicated by blue (red) hues. d) A schematic illustrates how perturbations can trigger small-to-medium or large earthquakes depending on E^{res}.

To visualize this, Figure 1c shows the variation in magnitude ΔM_W relative to residual energy. This indicates that the variation in M_W is small (large) when E^{res} is high (low). This supports the notion that there is a more restricted range of possible earthquakes when the residual energy in the fault is higher. Figure 1d schematically depicts this concept: a fault with a small E^{res} can generate earthquakes of magnitudes M_{W1} (blue area) and M_{W2} (orange area), whereas in the case of a large E^{res}, only earthquakes of magnitude M_{W3} (red area) can be generated, which is larger than both M_{W1} and M_{W2}.

3. Simulations

3.1 Heterogeneous Energy-Based method

The heterogeneous energy-based method (HE-Bm) posits that seismic rupture propagation is governed by the heterogeneous distribution of residual energy (Venegas-Aravena, 2023). This model suggests that rupture velocity and slip magnitude at each point on the fault are directly correlated with the residual

200 energy. Consequently, regions with high residual energy are more prone to
201 experiencing large slip u_f and high rupture velocities v_r, which can potentially
202 lead to larger magnitude earthquakes. Thus, the relation between slip and
203 residual energy is $u_f \propto E^{res}$.

204 According to the framework of HE-Bm, E^{res} can be linked to the distribution of
205 interseismic coupling on a fault through the concept of available energy, while
206 fault geometry is related to residual energy via fracture energy (Venegas-Aravena
207 and Cordaro, 2023a). The two-dimensional fractal dimension D of natural
208 fractures have been determined to be ~2.3 (Huang et al., 1992). Consequently,
209 due to the proportional relationship between the fracture energy G_C and the
210 geometric variations of the fracture (e.g. Xie,1993), it is expected that G_C will also
211 possess a fractal dimension of 2.3.

212

213 **3.2 Ruptures in a single distribution of G_C**

214 Figure 1a presents an exemplar G_C distribution exhibiting a fractal dimension of
215 2.3. The strike and depth are 700 km and 150 km respectively. The spacing is
216 349.5 m for the strike and 371.6 m for the depth. This distribution was constructed
217 through the interpolation of random values, employing the methodology outlined
218 by Chen and Yang (2016). Given the established inverse correlation between
219 elevated G_C values and rupture size (Renou et al., 2022), attributed to the self-
220 arresting nature of ruptures induced by energy depletion, the central region
221 (depicted in blue in Figure 1a) was intentionally constrained to be three orders of
222 magnitude less than the peripheral regions (rendered in red). Note that the arrest
223 of ruptures due to geometric changes (fracture energy) has also been observed

in real faults (e.g., Padilla et al., 2024). Consequently, ruptures are invariably localized within the lower G_C value domains (represented by the blue hues in Figure 1a). As coupling seems to be related to stress (Wallace et al., 2012), this implies that for a given level of stress on a fault, it is the fault roughness that primarily determines residual energy. Smoother faults exhibit lower fracture energy, resulting in reduced resistance to rupture initiation and, consequently, larger rupture events. Conversely, rougher faults present higher fracture energy, limiting residual energy and thus constraining rupture size.

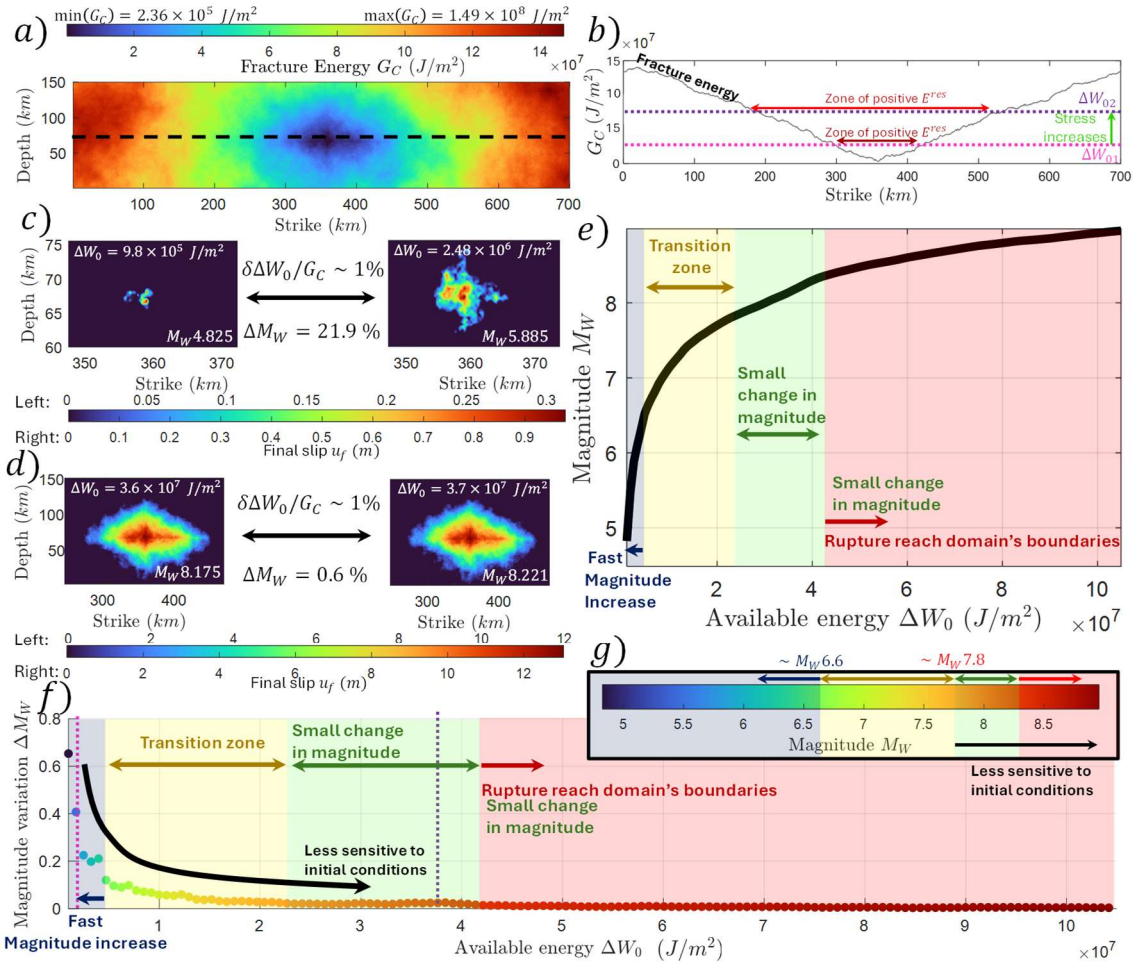

Figure 2: a) Example of fracture energy distribution with D=2.3, where the central region has low values, and the edges have high values. b) Fracture

energy profile corresponding to the segmented black line in a). Magenta and purple segmented lines indicate two levels of available energy ΔW_0. Dark red and red double arrows indicate the size of positive E^{res}, potentially corresponding to rupture size. c) and d) shows the final slip distributions for conditions of low and high available energy, respectively. c) reveals larger changes in magnitude than those shown in d). e) The relationship between moment magnitude and ΔW_0 is shown. The gray region highlights a rapid increase in magnitude with increasing ΔW_0, while the yellow and green zones show a decreasing rate of increase. The red zone indicates ruptures that reach the fault edges. f) The variation of magnitude with available energy for different values of the parameter ΔW_0 is shown. Lower values of ΔW_0 result in larger changes in magnitude. g) The color map used in f), which indicates the sensitivity of earthquakes to initial conditions: blue for smaller earthquakes (Mw~6.6), yellow for a transition region (Mw between 6.6 and 7.8), and red for larger earthquakes (Mw > 7.8) that are less sensitive.

Equivalently, for a given fracture energy distribution, the residual one will be determined by the amount of available energy. This example is shown in Figure 1b. The black curve corresponds to a trace indicated by the black segmented line in Figure 1a. The minimum value is $G_C = 2.36 \times 10^5\, J/m^2$, which is found approximately at the midpoint of the fault (strike of 350 km). These values of G_C tend to increase towards the strike equal to zero km and equal to 700 km. The segmented magenta and purple lines represent two uniform distributions of available energy, ΔW_{01} and ΔW_{02}, respectively. In this case, ΔW_{02} is greater than

ΔW_{01}, indicating that the first case has a smaller amount of accumulated stress on the fault than the second case. The dark red double arrow would indicate the zone with positive residual energy given the level of ΔW_{01}, which is equivalent to a potential rupture zone. The red double arrow indicates the zone of positive residual energy given a higher accumulated stress (given by ΔW_{02}). This zone is wider than the region marked by the dark red arrow, highlighting the presence of larger ruptures promoted by high stress values throughout the crustal volume. The increase of available energy also translates into changes in earthquake magnitudes. For instance, Figure 2c illustrates two ruptures initiated with similar available energy ($\sim 10^6\, J/m^2$), representing a one percent variation relative to the maximum fracture energy. This excess in available energy defines the positive residual energy area (rupture area A), which can be related to the seismic moment M_0 through the empirical relationship $M_0 = \mu C_2 A^{3/2}$, where μ is the shear modulus with a value of $4 \times 10^{10} Pa$ and C_2 is a dimensionless constant equal to 3.8×10^{-5} (Leonard, 2010). The small variation available energy results in a ~22% increase in earthquake magnitude (from M_W~4.8 to M_W~5.9). Conversely, when the available energy is higher ($\sim 3.6 \times 10^7\, J/m^2$), a similar 1% increase produces earthquakes with nearly identical magnitudes (M_W~ 8.2 representing a variation smaller than 1%, as shown in Figure 2d), suggesting that faults with higher residual energy yield similar magnitude earthquakes.

The dependence of magnitude on available energy is depicted in Figure 2e. This figure shows 140 simulations with different values of ΔW_0. A significant increase in magnitude is observed for low available energy values, indicated by the blue region. In this region, a small increase in ΔW_0 (less than 10 MJ/m^2) can elevate an earthquake from magnitudes less than 5 to approximately M_W6.6. The yellow

and green regions show a less pronounced increase in magnitude compared to the blue region. The red range represents events where the ruptures approach the fault boundaries. The magnitude change in this region appears unaffected by fault boundary influences. Figure 2f quantifies these variations, revealing that the blue region experiences ΔM_W values close to 0.7, while the green and red regions show negligible changes. The color map in Figure 2g corroborates these findings, with earthquakes smaller than M_W6.6 predominantly falling within the blue region and larger earthquakes (M_W larger than M_W7.8) exhibiting minimal sensitivity to variations in ΔM_W.

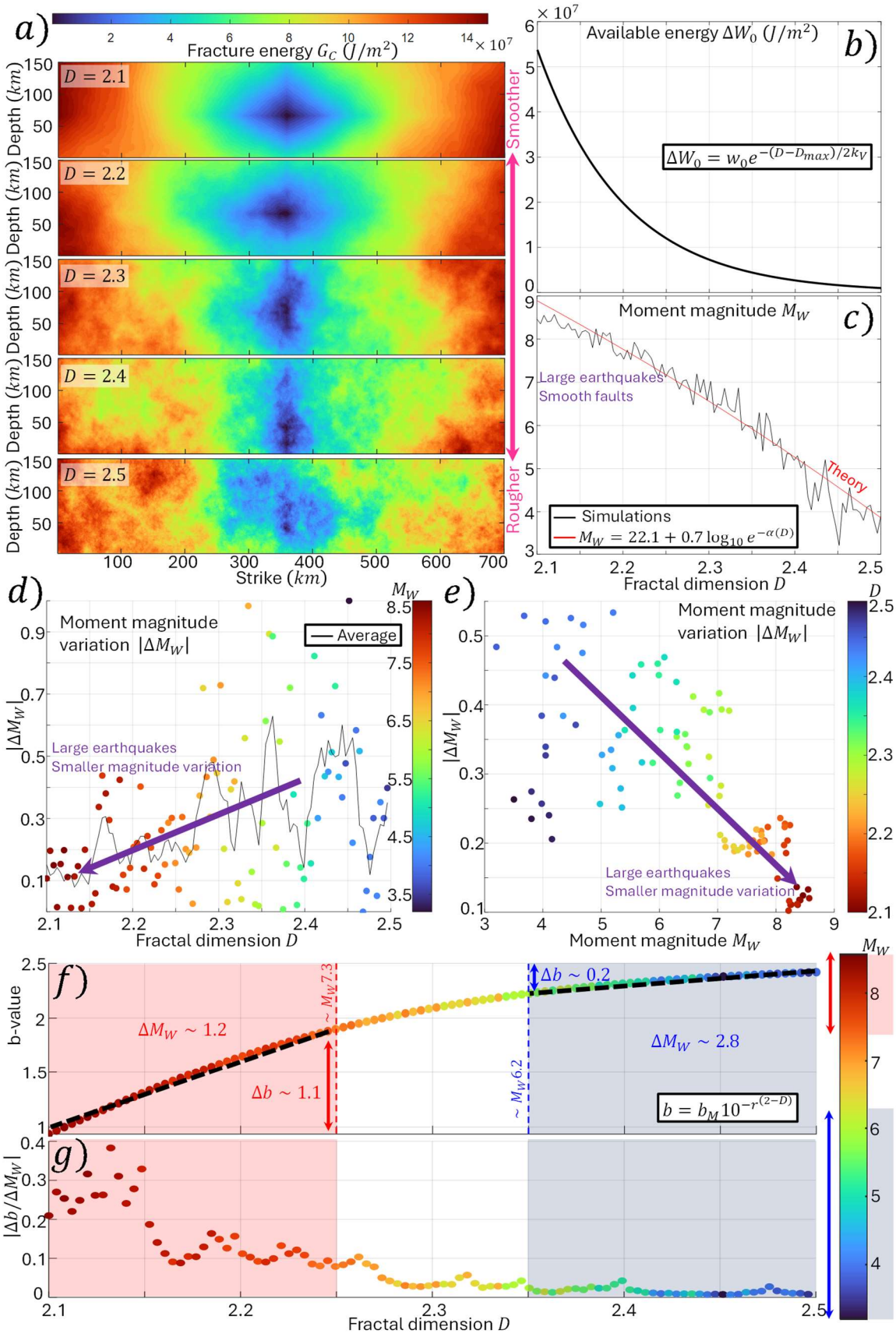
a)
Fracture energy G_C (J/m^2)
$\times 10^7$
$D = 2.1$
$D = 2.2$
$D = 2.3$
$D = 2.4$
$D = 2.5$
Depth (km)
Strike (km)
Smoother
Rougher
b)
Available energy ΔW_0 (J/m^2)
$\Delta W_0 = w_0 e^{-(D-D_{max})/2k_V}$
c)
Moment magnitude M_W
Large earthquakes
Smooth faults
Theory
Simulations
$M_W = 22.1 + 0.7 \log_{10} e^{-\alpha(D)}$
Fractal dimension D
d)
Moment magnitude variation $|\Delta M_W|$
Average
Large earthquakes
Smaller magnitude variation
Fractal dimension D
e)
Moment magnitude variation $|\Delta M_W|$
Large earthquakes
Smaller magnitude variation
Moment magnitude M_W
f)
b-value
$\Delta M_W \sim 1.2$
$\Delta b \sim 1.1$
$\sim M_W 7.3$
$\Delta b \sim 0.2$
$\Delta M_W \sim 2.8$
$\sim M_W 6.2$
$b = b_M 10^{-r(2-D)}$
g)
$|\Delta b / \Delta M_W|$
Fractal dimension D

295

Figure 3: a) Fracture energy of a fault with different fractal dimension (D) values. The distribution becomes rougher as D increases. b) There is an exponential relationship between available energy and D. As D decreases, the available energy increases exponentially. c) The relationship between moment magnitude and D is shown. The simulated data is represented by the black curve, and the theoretical prediction by Venegas-Aravena and Cordaro (2023a) is shown in red. d) and e) show the relationship between fractal dimension, moment magnitude, and magnitude variation. The purple arrow indicates that in both figures, low values of D are associated with high-magnitude earthquakes and small magnitude variations. That is, a small change in D, when ΔW_0 values are high, almost always generates similar large earthquakes. When ΔW_0 values are low, there is a greater variation in magnitude. f) Relationship between b-value and D. There is a greater decrease in the b-value when there are larger earthquakes. g) Variation of the b-value with changes in M_W. This variation is greater when D is lower.

3.3 Ruptures with different G_C

While natural faults can be characterized by a fractal dimension of approximately 2.2 (e.g. Kagan, 1991), variations in this value are possible. To investigate the impact of fractal dimensions on fracture energy, 100 simulations were conducted with fractal dimensions ranging from 2.1 to 2.5. Figure 3a illustrates examples of fault geometries with fractal dimensions of 2.1, 2.2, 2.3, 2.4, and 2.5, respectively, where maximum and minimum G_C values are consistent with Figure 2a. In these

simulations, lower G_C values are maintained at the fault center and higher values at the edges. As shown in Figure 3a, the distribution of G_C becomes smoother as the fractal dimension approaches 2.1.

As suggested by Venegas-Aravena and Cordaro (2023a), ΔW_0 is inversely related to D, with the specific relationship being $\Delta W_0 \sim e^{-D/2k_V}$. Therefore, any change in G_C must be accompanied by a corresponding change in ΔW_0. Figure 3b visualizes this relationship using parameter values of $w_0 = 9.8436 \times 10^5\ J/m^2$, $D_{max} = 2.5$ and $k_V = 0.05$. These values yield a range of ΔW_0 consistent with the previous section, ensuring that ΔW_0 is sufficiently large to allow for rupture initiation but not so large as to be influenced by domain boundaries. The figure clearly demonstrates that lower values of D are associated with higher values of ΔW_0, indicating smoother spatial distributions of G_C. The magnitude of these ruptures also varies as a function of D. In Figure 3c, the red curve represents the theoretical relationship proposed by Venegas-Aravena and Cordaro (2023a), given by $M_W \sim \log_{10} e^{-\alpha}$, where $\alpha = pD/k_V$ and $p = 3/(5 - D)$. The observed magnitudes, depicted by the black curve, align well with the theoretical values. However, a higher variability in magnitude $|\Delta M_W|$ is observed for larger values of D (greater than 2.4), while lower values of D (less than 2.3) exhibit lower variability. This variation is visualized in Figure 3d, where the color map indicates magnitude. The black curve in Figure 3d represents a 5-point moving average of $|\Delta M_W|$, with the purple arrow highlighting the trend towards lower magnitude variability for smaller values of D. Figure 3e explicitly shows the relationship between M_W and its average variability (in this case a 10-point moving average), with the color map indicating D values. As the purple arrow suggests, there is an inverse correlation between M_W and its average variability, where earthquakes

with magnitudes less than $M_W \sim 5$ can exhibit magnitude differences greater than $0.5M_W$. In contrast, for earthquakes with magnitudes greater than $M_W \sim 8$, this variability decreases to approximately $0.1M_W$.

3.4 Chaos and b-value

Both laboratory and field studies have shown a negative correlation between the b-value, which quantifies the frequency of earthquakes of different magnitudes in each region and increasing stress levels. This leads to a decrease in the b-value and may be associated with large magnitude earthquakes (Scholz, 2015; Dong et al., 2022). Studies have established a theoretical link between the b-value and fractal dimension, suggesting that lower b-values correspond to lower D values and vice versa (Aki, 1981; Venegas-Aravena and Cordaro, 2023b). Specifically, this relationship is expressed as $b - value = b_M 10^{-r^{(2-D)}}$, where b_M is 2.5 and r is a constant between 10^3 and 10^4 (in this study, r is set to medium value 5000 for simulations). This law is illustrated in Figure 3f. The color map indicates earthquake magnitudes, with blue transparency representing events from $M_W \sim 3.4$ to $M_W \sim 6.2$, corresponding to a D variation of 1.5. The magnitude variation within this zone is $\Delta M_W \sim 2.8M_W$, while the b-value decrease is $\Delta b \sim 0.2$. Red transparency indicates the same variation of D, but with earthquakes ranging from $M_W \sim 7.3$ to $M_W \sim 8.5$, corresponding to a $\Delta M_W \sim 1.2$ and a $\Delta b \sim 1.1$ decrease. The reduction in the rate of change of the b-value with respect to magnitude is clearly displayed in Figure 3g. The blue transparent area emphasizes a region where the absolute value of the b-value remains relatively constant, even as the magnitude of earthquakes fluctuates. It is important to note

that a 5-point moving average was applied to the data. This suggests that the b-value is less sensitive to changes when the fault system predominantly generates smaller earthquakes. In contrast, the red transparent area reveals a more pronounced relationship between b-value and magnitude, with the b-value fluctuating more rapidly as the magnitude increases. These results imply that a more abrupt decrease in the b-value is associated with smaller changes in magnitude but, likely, also with changes in fault conditions leading to less chaotic behavior.

4. A reality check: comparison with seismicity in Southern California

We have already compared our theoretical predictions with the output of dynamic simulations of earthquakes; here we make a reality check with the statistical properties of seismic catalogs. Specifically, we validate the compatibility of the relationship $b - value = b_M 10^{-r^{(2-D)}}$, between the b-value of the Gutenberg-Richter law and the fractal dimension of faulting. Since it is not possible to directly investigate the fractal properties of faults, we calculate the fractal dimension of hypocenters (hereafter referred as D), which are expected to be distributed within a subset of the fracture network; hence, D is equal or lower than the value for the fault system. Nevertheless, even with different coefficients (b_M and r), the empirical law of the b-value follows the same trend because seismic events are supposed to occur throughout the whole investigated crustal volumes. Thus, we specify that we are not interested either in assessing the true fractal dimension of the networks of faults hosting seismicity (an accurate estimation is not feasible) nor the true fractal dimension of seismic events in their long-term behavior (which

would require much longer catalogs than available nowadays and accurate declustering). Here, our goal is just the observational validation of the mathematical relationship $b - value = b_M 10^{-r^{(2-D)}}$. It requires a high-quality relocated seismic catalog produced by a roughly uniformly distributed network of seismic stations (i.e., uniform completeness magnitude). Both the background and triggered components are considered, otherwise the spatial variations of the b-value and fractal dimension vanish preventing any investigation of their relationship with the available catalogs.

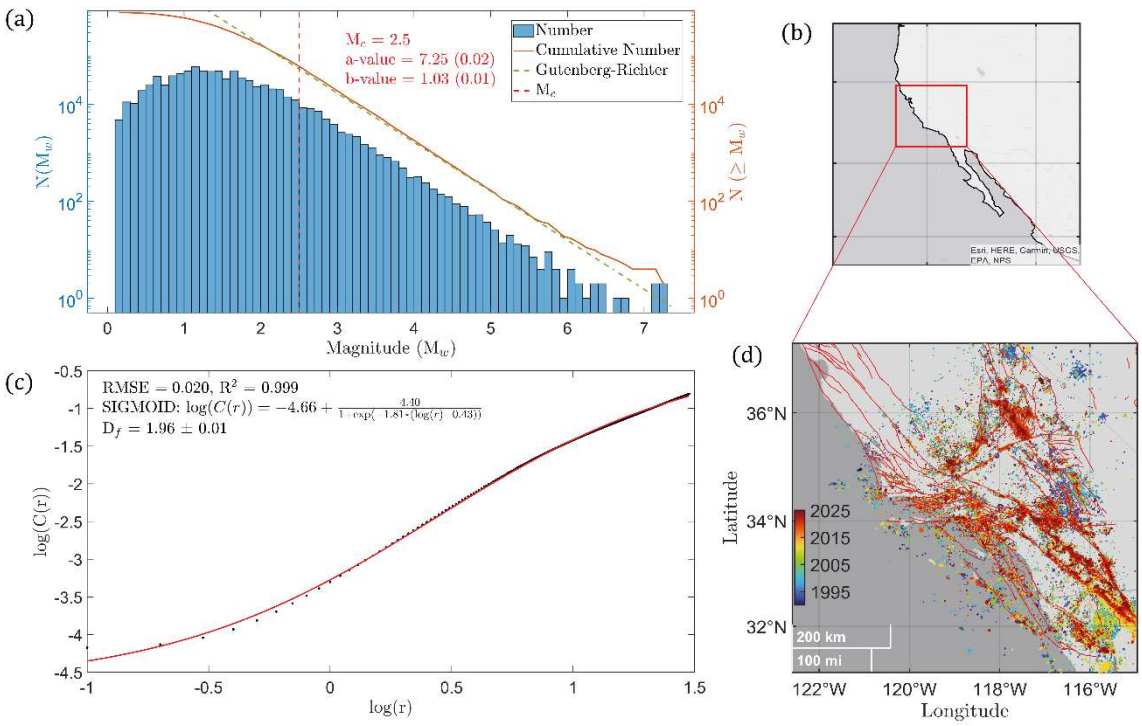

Figure 4: Seismicity in Southern California (SCEC Catalog, 1990-2025, latitude 31°-37° N, longitude 115°-122° W, depth lower than 30 km). (a) Frequency-magnitude distribution of seismicity, the completeness magnitude is highlighted by the red vertical dashed line. In (b) and (d) is the map with the spatial distribution of seismicity. (c) log-log representation of

the correlation function vs the threshold radial distance (km). The plot shows a range of scales where the curve is well approximated by a line, i.e., hypocenters follow a fractal distribution in space.

We analyze the shallow crustal seismicity (depth lower than 30 km) in Southern California between 1/1/1990 and 20/1/2025 listed in the Waveform Relocated Earthquake Catalog for Southern California (Hauksson et al., 2012). A visual representation of seismicity considered in this study is given in Figure 4a, b and d. The catalog is divided into several squared regions. The number and selection procedure used to define the structure of the subsets do not significantly affect the final output provided that the fractal probability and the b-value be investigated only for regions with at least 500 events to get stable and reliable results. Only events above the completeness magnitude are considered, with Mc = 2.5. It is estimated according to the EMR method (Woessner and Wiemer, 2005). Since short-term aftershocks incompleteness (STAI) after the occurrence of major events is still present even if a great part of the catalog contains reliable information, the b-value is calculated using the b-positive algorithm (van der Elst, 2021) with the b-more positive correction (Lippiello and Petrillo, 2024) to avoid bias. The uncertainty of the b-value is found using bootstrapping over 100 simulations with acceptance probability equal to 0.5. The fractal dimension of the hypocenters is measured using the Grassberger and Procaccia algorithm (Grassberger and Procaccia, 1983). Here, we introduce a new method to remove possible sources of bias in its estimation due to the arbitrary selection of the lower and upper cut-offs for the linear region in the log-log plot. The curve of the correlation function $C(r)$ as a function of the threshold radius r is fitted using the

sigmoid function $y = y_0 + k/(1 + e^{-\alpha x})$, where $y = \log\big(C(r)\big)$ and $x = \log(r)$, while k, alpha and y_0 are left as free parameters, so that the fractal dimension (i.e., the derivative of the sigmoid in its symmetry saddle point) is given by $D = k\alpha$. The uncertainty is calculated by propagating the fit errors of k and α. The estimation of the fractal dimension of hypocenters for the whole catalog is in Figure 4c. The analysis performed over a wide range of possible grids (both uniformly spaced and nested according to the number of seismic events within them) shows that the b-value and the fractal dimension of hypocenters are positively correlated; moreover, the curve $b - value = b_M 10^{-r^{(2-D)}}$ provides a good fit of the relationship between b and D, in agreement with our theoretical prediction. The output of our investigation is summarized in Figure 5.

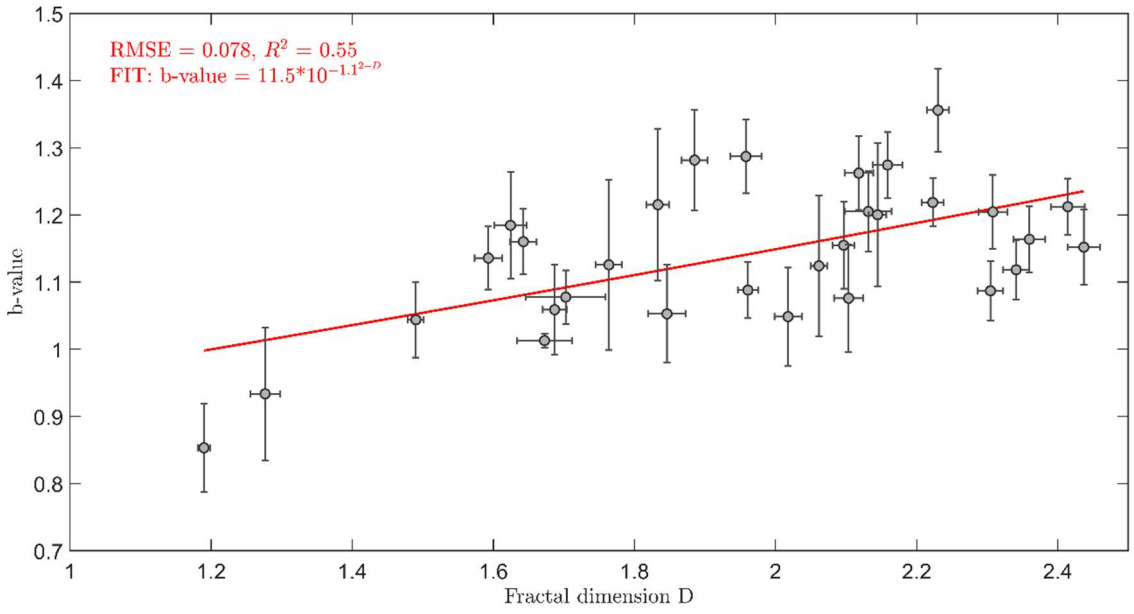

Figure 5: b-value vs fractal dimension of hypocenters (D) in Southern California. The b-value of the Gutenberg-Richter law is found to be positively correlated with the fractal dimension of hypocenters in Southern

California (SCEC Catalog, Hauksson et al., 2012) coherently with previous literature on the topic. The plot represents shallow crustal seismicity from 1/1/1990 to 20/1/2025 (depth lower than 30 km) in between latitude 31°-37° N and longitude 115°-122° W and above the completeness magnitude Mc = 2.5. Error bars represent 1σ uncertainty. The b-value is estimated using the b-more-positive approach, while the fractal dimension of hypocenters is found by applying the Grassberger & Procaccia algorithm (Grassberger and Procaccia, 1983). The red line is the output of the non-linear fit b-value = $b_M 10^{-r^{2-D}}$ whose trend is predicted in our model and derived in Venegas-Aravena and Cordaro, 2023b.

5. Discussions

The chaotic nature of earthquakes has been a subject of intense debate within the scientific community (e.g., Scholz, 1990; Huang and Turcotte, 1992; Goltz, 1997; Vieira, 1999; Yılmaz et al., 2023). Traditionally, earthquakes have been considered highly unpredictable due to the complexity of the processes involved in fault rupture (e.g., Geller et al., 1997; Kagan 1997). However, a growing body of research, spanning conceptual frameworks, crustal stress, thermodynamics, artificial intelligence, and GNSS measurements, suggests that fault stability may be investigated, with a potential influence on precursory activity, may be achieved (e.g., Wyss, 1997; Crampin and Gao, 2010; Posadas et al., 2021; Bhatia et al., 2023; Bletery and Nocquet 2023; Devi et al., 2024), especially in the case of larger magnitude seismic event (Kaveh et al., 2024). In this study, we propose a novel perspective, grounded in multi-scale thermodynamics, suggesting that the

chaotic nature of earthquakes may be modulated by the residual energy stored within faults volumes (Venegas-Aravena and Cordaro 2023a). These primarily theoretical developments suggest that as the thermodynamic fractal dimension (D) decreases, the residual energy in the system increases. This correlation is further supported by the framework presented in Section 2, where we demonstrate that a higher residual energy is linked to a lower sum of Lyapunov exponents Λ (red regions in Figure 1b), a hallmark of reduced chaoticity. Consequently, earthquakes with higher residual energy exhibit more deterministic behavior, as larger magnitude earthquakes (lower Λ) show a smaller change in magnitude per unit of residual energy (Figure 1c). This suggests that these earthquakes are less susceptible to the exponential growth of small perturbations, a hallmark of chaotic systems.

Section 3 evaluates the proposed hypothesis through numerical simulations of kinematic rupture using the HE-B method. This method has been effective in modeling self-arrested earthquakes that comply with observational constraints, such as the asperity criterion of Somerville et al. (1999), which links the zone of high slip (known as asperity) to the release of a large amount of seismic energy. The results obtained show a clear relationship between residual energy and the variability in earthquake magnitude. For instance, the blue zone in Figure 2e demonstrates that smaller earthquakes (M_W < 6.6) exhibit a high sensitivity to variations in available energy. This means that small increases in available energy can lead to significant increases in the magnitude of the resulting earthquake, as evidenced by the high values of ΔM_W and the regions of high magnitude variability (transparent blue zone in Figure 2f). Specifically, this indicates that a 1% increase in available energy can result in an increase in the

magnitude of the resulting earthquake greater than $0.5M_W$. In other words, when a fault has a specific low value of available energy (e.g., $0.1 \times 10^7 J/m^2$) and has the potential to generate a magnitude $M_W = 5$ earthquake, it can produce a larger earthquake ($M_W = 5.5$) or a smaller one ($M_W = 4.5$) if the available energy is slightly increased or decreased. In contrast, larger earthquakes (M_W > 7.8) show a notable lack of sensitivity to changes in available energy (transparent green and red zones in Figure 2f). These zones indicate that a slight increase or decrease in available energy does not produce significant changes in the magnitude of the resulting earthquake. This low sensitivity demonstrates less chaotic behavior in the simulations, where larger earthquakes are more predictable and less influenced by small perturbations. This also suggests that these larger events may also be more predictable. In line with this, analyses conducted in seismic rupture simulations with a rate-and-state friction law on simple faults (Kaveh et al., 2024) are consistent with the results shown in this work, which is based on the distribution of residual energy. An interesting aspect of the work by Kaveh et al. (2024) comes from the threshold above which predictions can be made. They observed that it was possible to make forecasts of earthquakes with magnitudes greater than approximately $M_W 6.9$. In contrast, Figures 2e and 2f indicate that the variation in magnitude due to a change in available energy begins to be less than $0.1M_W$ when earthquakes begin to have magnitudes greater than $M_W 6.6$ (transparent yellow zone). This suggests a similar threshold for predictability in both studies.

To further assess the link between residual energy and chaos in seismic activity, numerical simulations were performed varying both the fracture energy distribution and the system's available energy, in accordance with Equation 5.

523 The findings strongly corroborate the proposed hypothesis. Figure 3c, for
524 example, demonstrates an excellent agreement between the simulated
525 magnitude-parameter D relationship (black curve) and the theoretically predicted
526 one (Equation 2, red curve), affirming the established theoretical connection
527 between parameter D, residual energy, and simulated earthquake magnitudes.
528 Additionally, Figures 3d and 3e corroborate the trend observed in the earthquakes
529 of Figure 2: larger magnitude earthquakes exhibit a smaller variation in their
530 magnitude, suggesting a lower degree of chaos in these events. To gain further
531 credibility, a parameter more commonly used in seismology was needed. The b-
532 value of the Gutenberg-Richter law has traditionally been used as an indicator of
533 the relative occurrence rate of earthquakes of different magnitudes (Ito and
534 Kaneko, 2023; Lacidogna et al., 2023). In this study, the relationship between the
535 b-value and the degree of chaos in seismicity has been explored. In particular,
536 Figure 3f shows that the b-value decreases more abruptly for earthquakes with
537 magnitudes greater than $M_W 7.3$ (red zone), indicating a decrease in the
538 occurrence rate of smaller earthquakes relative to larger ones. This behavior is
539 associated with b-value changes on the order of 0.4 and suggests a less chaotic
540 regime. On the other hand, for earthquakes with magnitudes less than $M_W 6.3$
541 (blue zone), the b-value exhibits less pronounced changes, indicating a greater
542 variability in the occurrence rate of earthquakes of different magnitudes, and
543 therefore, a more chaotic regime. This relationship between the b-value and
544 seismic chaos is consistent with the interpretation of parameter D. Low D values
545 (associated with higher-magnitude earthquakes) imply a more homogeneous
546 distribution of residual energy over a larger area within faults, thereby reducing
547 the probability and number of smaller events. Consequently, the ratio of large to

small events, known as the b-value, is directly influenced by D. Therefore, it can be argued that a typical decrease in the b-value (e.g., Rivière et al., 2018; Sharon et al., 2022; Chan et al., 2024) is a measure of the chaos of a system, supporting the notion that low b-values are associated with imminent larger magnitude earthquakes, coherently with previous research (e.g., Gulia and Wiemer, 2019).

We also prove the theoretical relationship between the b-value and fractal dimension $b - value = b_M 10^{-r^{(2-D)}}$, also supporting the idea that large earthquakes tend to occur within networks with low fractal dimensions (i.e., along major faults). See Figure 5 for the output in the case of the SCEC Catalog in Southern California (1990-2025). Observations show good agreement with theory and, even though with relatively large uncertainties, are statistically robust. It is important to note that, according to Venegas-Aravena and Cordaro (2023b), the case where b-value and D are approximately proportional can be obtained, as shown in Figure 5. The direct effect of the fractal dimension of faulting on the maximum magnitude is more difficult to observe since large earthquakes are rare events and the available seismic catalogs only contain a few cases, if any, of events with the largest expected magnitude for each fault system, preventing a reliable analysis. Moreover, the results would be rescaled for the size of the largest seismogenic source in each fault network, which is tricky to estimate. Conversely, the b-value can nowadays be evaluated by robust and unbiased estimators. This is the reason why we choose to validate directly the relationship between b and D.

The analyses conducted in this study, which involves theoretical, numerical and observational data, contrast with the traditional view of earthquakes as highly chaotic systems. However, it is important to note that our proposal does not

dismiss the role of chaos in seismic rupture dynamics. Rather, it suggests that the chaotic behavior may be modulated by the amount of residual energy stored in the fault. In other words, when residual energy is high, the probability of releasing all that energy in a sudden event increases due to the coalescence of different fault segments ready to nucleate or that can be dynamically activated during the coseismic phase. Conversely, when residual energy is low, the fault has more options for releasing that energy, which can lead to seismic ruptures of varying sizes. Our findings have significant implications for understanding the precursor seismicity, known as foreshocks (e.g., Lippiello et al., 2019; Bolton et al., 2023). If we can accurately quantify the residual energy in a fault, we may be able to estimate the probability of large magnitude earthquakes and assess their destructive potential.

This is particularly significant as recent research indicates that approximately half of large-magnitude seismic events may be preceded by precursor seismic activity, although the magnitude difference between foreshocks and mainshocks does not appear to be substantial (Wetzler et al., 2023). This suggests that states of higher energy preferentially evolve into large earthquakes. These states are associated with a greater amount of available energy, which is directly related to stress. Here, it is important to note that low values of D also indicate an accumulation of stress in localized areas (Venegas-Aravena et al., 2022). Geodetic measurements have confirmed this accumulation of localized stresses between earthquakes of magnitudes greater than $M_W 7$ (Kato and Ben-Zion, 2020). Additionally, foreshocks also appear to be related to the geometric conditions of faults (e.g., McLaskey and Kilgore, 2013; Cattania and Segall, 2021), which can be incorporated into the residual energy through fracture

energy. Subsequently, residual energy can be used to estimate the physics of seismic precursors. For instance, it has been estimated that foreshocks may not be reliable when estimating the probability of subsequent mainshocks (Zaccagnino et al., 2024). Here, residual energy in the context of multi-scale thermodynamics can offer two explanations for the lack of clarity regarding foreshocks. Firstly, foreshock-type activity should arise as a stress perturbation, which, when considering a state of residual energy, can trigger events of different magnitudes but within a range of magnitudes close to that of the potential future mainshock. However, the magnitude of these foreshocks can be chaotic, limiting the ability to conduct statistical analyses and thus declaring them as foreshocks in real-time measurements. Secondly, the increase in residual energy implies a lower variability in the magnitude of earthquakes, in agreement with Lippiello et al., 2024. This suggests that when residual energy may be very high in a fault, stress perturbation has higher chances to trigger large earthquakes, limiting the existence of foreshocks. That is, the probability that larger earthquakes are affected or associated with foreshocks could decrease with an increase in the magnitude of the mainshock.

Here, one way to associate foreshocks with large magnitude mainshocks is if the rupture area of a foreshock reaches a zone of the fault with very high residual energy, which could be seen as a perturbation leading to a single large subsequent earthquake. This scenario could occur in the so-called "Mogi Doughnut" of subduction zones (Mogi, 1969), where the shallowest zones of the plate interface accumulate large amounts of energy while most seismicity occurs at deeper locations with lower accumulated energy (Schurr et al., 2020).

The findings and interpretation carried out in this work agree with recent modeling and observational findings in the literature (e.g., Longobardi et al., 2024; Nielsen, 2024) and could also influence future research, which may focus on developing methods to directly measure residual energy in natural faults, creating more sophisticated models that incorporate parameter D and allow for the simulation of the evolution of residual energy over time. Finally, exploring the implications of our results for seismic risk assessment and the design of earthquake-resistant structures.

6. Conclusions

The results obtained in this study suggest that the chaotic behavior of earthquakes can be modulated by the amount of residual energy stored in the fault. Our findings indicate that larger earthquakes, associated with higher residual energy, exhibit less chaotic behavior. This new perspective challenges traditional conceptions about the nature of earthquakes and opens new avenues of research in seismology. While these results are promising, further research is required to confirm and deepen our findings. Specifically, methods need to be developed to directly measure residual energy in natural faults and to construct more sophisticated models that incorporate the parameter D. This research will allow us to advance our understanding of the mechanisms governing the generation and propagation of earthquakes and pave the way for a better assessment and mitigation of seismic risk.

Data and Code Availability

Data and codes are available upon reasonable requests to both the authors.

Acknowledgment

The authors wish to thank the editor for handling the manuscript and reviewers whose comments and suggestions greatly improved the first version of the paper. Discussions with Valeria Becerra-Carreño, Enrique G. Cordaro, Matteo Picozzi and Didier Sornette have been inspiring for the work.

Competing interests

The authors declare no competing interests.

References

Aki K (1981) A probabilistic synthesis of precursory phenomena, in Earthquake Prediction: An International Review, pp. 566–574, eds Simpson D.W. Richards P. G., AGU, Washington, DC

Aksoy CG, Chupilkin M, Koczan Z, Plekhanov A (2024) Unearthing the impact of earthquakes: A review of economic and social consequences. Journal of Policy Analysis and Management 2024(1): 1-22. https://doi.org/10.1002/pam.22642

667 Barras F, Thøgersen K, Aharonov E, Renard F (2023) How Do Earthquakes
668 Stop? Insights From a Minimal Model of Frictional Rupture. Journal of
669 Geophysical Research 128(8): 1-22. https://doi.org/10.1029/2022JB026070

670

671 Bhatia M, Ahanger TA, Manocha A (2023) Artificial intelligence based real-time
672 earthquake prediction. Engineering Applications of Artificial Intelligence 120(1):1-
673 14. https://doi.org/10.1016/j.engappai.2023.105856

674

675 Bletery Q, J-M Nocquet (2023) The precursory phase of large earthquakes.
676 Science 381(6655): 297-301. https://doi.org/10.1126/science.adg2565

677

678 Bolton DC, Marone C, Saffer D, Trugman DT (2023) Foreshock properties
679 illuminate nucleation processes of slow and fast laboratory earthquakes. Nature
680 Communications 14(3859): 1-11. https://doi.org/10.1038/s41467-023-39399-0

681

682 Cattania C, Segall P (2021) Precursory Slow Slip and Foreshocks on Rough
683 Faults. Journal of Geophysical Research 126(4): 1-20.
684 https://doi.org/10.1029/2020JB020430

685

686 Chan C-H, Kao J-C, Chen D-Y (2024) Spatial–temporal variations of b-values
687 prior to medium-to-large earthquakes in Taiwan and the feasibility of real-time

precursor monitoring. Earth Planets Space 76(119): 1-14. https://doi.org/10.1186/s40623-024-02065-w

Chen Y, Yang H (2016) Numerical simulation and pattern characterization of nonlinear spatiotemporal dynamics on fractal surfaces for the whole-heart modeling applications. The European Physical Journal B 89(181): 1-16. https://doi.org/10.1140/epjb/e2016-60960-6

Christensen DH, Beck SL (1994) The rupture process and tectonic implications of the great 1964 Prince William Sound earthquake. Pure and Applied Geophysics 142(1): 29–53. https://doi.org/10.1007/BF00875967

Colavitti L, Lanzano G, Sgobba S, Pacor F, Gallovič F (2022) Empirical Evidence of Frequency-Dependent Directivity Effects From Small-To-Moderate Normal Fault Earthquakes in Central Italy. Journal of Geophysical Research 127(6):1-24. https://doi.org/10.1029/2021JB023498

Crampin S, Gao Y (2010) Earthquakes can be stress-forecast. Geophysical Journal International 180(3): 1124–1127. https://doi.org/10.1111/j.1365-246X.2009.04475.x

709 Devi DR, Govindarajan P, Venkatanathan N (2024) Towards real-time earthquake
710 forecasting in Chile: Integrating intelligent technologies and machine learning.
711 Computers and Electrical Engineering 117(1): 1-15.
712 https://doi.org/10.1016/j.compeleceng.2024.109285

713

714 Dong L, Zhang L, Liu H, Diu K, Liu X (2022) Acoustic Emission b Value
715 Characteristics of Granite under True Triaxial Stress. Mathematics 10(3):1-16.
716 https://doi.org/10.3390/math10030451

717

718 Erickson BA, Birnir B, Lavallée D (2011) Periodicity, chaos and localization in a
719 Burridge–Knopoff model of an earthquake with rate-and-state friction.
720 Geophysical Journal International 187(1): 178–198.
721 https://doi.org/10.1111/j.1365-246X.2011.05123.x

722

723 Geller RJ, Jackson DD, Kagan YY, Mulargia F (1997) Earthquakes Cannot Be
724 Predicted. Science 275(5306): 1616-1617.
725 https://doi.org/10.1126/science.275.5306.1616

726

727 Goltz C (1997) Fractal and Chaotic Properties of Earthquakes. Lecture Notes in
728 Earth Sciences 77(1): 3-164. https://doi.org/10.1007/BFb0028316

729

730 Grassberger P, Procaccia I (1983) Measuring the strangeness of strange
731 attractors. Physica D: nonlinear phenomena, 9(1-2), 189-208.
732 https://doi.org/10.1016/0167-2789(83)90298-1

733

734 Gualandi A, Faranda D, Marone C, Cocco M, Mengaldo G (2023) Deterministic
735 and stochastic chaos characterize laboratory earthquakes. Earth and Planetary
736 Science Letters 604(1): 1-13. https://doi.org/10.1016/j.epsl.2023.117995

737

738 Gudmundsson A (2014) Elastic energy release in great earthquakes and
739 eruptions. Frontiers in Earth Science 2(1):1- 12.
740 https://doi.org/10.3389/feart.2014.00010

741

742 Gulia L, Wiemer S (2019) Real-time discrimination of earthquake foreshocks and
743 aftershocks. Nature, 574(7777), 193-199. https://doi.org/10.1038/s41586-019-
744 1606-4.

745

746 Hauksson E, Yang W, Shearer PM (2012) Waveform relocated earthquake
747 catalog for southern California (1981 to June 2011). Bulletin of the Seismological
748 Society of America, 102(5), 2239-2244. https://doi.org/10.1785/0120120010

749

750 Hoover WG, Posch HA (1994) Second-law irreversibility and phase-space
751 dimensionality loss from time-reversible nonequilibrium steady-state Lyapunov

752 spectra. Physical Review E 49(3):1913-1921.
753 https://doi.org/10.1103/PhysRevE.49.1913

754

755 Huang J, Turcotte DL (1990) Are earthquakes an example of deterministic chaos?
756 Geophysical Research Letters 17(3): 223-226.
757 https://doi.org/10.1029/GL017i003p00223

758

759 Huang SL, Oelfke SM, Speck RC (1992) Applicability of fractal characterization
760 and modelling to rock joint profiles. International Journal of Rock Mechanics and
761 Mining Sciences & Geomechanics Abstracts 29(2): 89-98.
762 https://doi.org/10.1016/0148-9062(92)92120-2

763

764 Huang J, Turcotte DL (1992) Chaotic seismic faulting with a mass-spring model
765 and velocity-weakening friction. Pure and Applied Geophysics 138(1): 569–589.
766 https://doi.org/10.1007/BF00876339

767

768 Iaccarino AG, Picozzi M (2023) Detecting the Preparatory Phase of Induced
769 Earthquakes at The Geysers (California) Using K-Means Clustering. Journal of
770 Geophysical Research 128(10): 1-18. https://doi.org/10.1029/2023JB026429

771

772 Ito R, Kaneko Y (2023) Physical Mechanism for a Temporal Decrease of the
773 Gutenberg-Richter b-Value Prior to a Large Earthquake. Journal of Geophysical
774 Research 128(12):1-21. https://doi.org/10.1029/2023JB027413

775

776 Kagan YY (1991) Fractal dimension of brittle fracture. Journal of Nonlinear
777 Science 1(1):1-16. https://doi.org/10.1007/BF01209146

778

779 Kahandawa KARVD, Domingo ND, Park KS (2018) Earthquake damage
780 estimation systems: Literature review. Procedia Engineering 212(1): 622-628.
781 https://doi.org/10.1016/j.proeng.2018.01.080

782

783 Kato A, Ben-Zion Y (2020) The generation of large earthquakes. Nature
784 Reviews Earth & Environment 2(1): 26–39. https://doi.org/10.1038/s43017-020-
785 00108-w

786

787 Kintner JA, Ammon CJ, Cleveland KM, Herman M (2018) Rupture processes of
788 the 2013–2014 Minab earthquake sequence, Iran. Geophysical Journal
789 International 213(3): 1898–1911. https://doi.org/10.1093/gji/ggy085

790

791 Kagan YY (1997) Are earthquakes predictable? Geophysical Journal
792 International 131(3): 505–525. https://doi.org/10.1111/j.1365-
793 246X.1997.tb06595.x

Kaveh H, Avouac JP, Stuart AM (2024) Spatiotemporal forecast of extreme events in a chaotic dynamical model of slow slip events. Geophysical Journal International, ggae417. https://doi.org/10.1093/gji/ggae417

Knopoff L (1958) Energy Release in Earthquakes. Geophysical Journal International 1(1): 44–52. https://doi.org/10.1111/j.1365-246X.1958.tb00033.x

Kossobokov, VG, Panza, GF (2020) A myth of preferred days of strong earthquakes?. Seismological Research Letters, 91(2A), 948-955.

Lacidogna G, Borla O, De Marchi V (2023) Statistical Seismic Analysis by b-Value and Occurrence Time of the Latest Earthquakes in Italy. Remote Sensing 15(21): 1-20. https://doi.org/10.3390/rs15215236

Leonard M (2010) Earthquake Fault Scaling: Self-Consistent Relating of Rupture Length, Width, Average Displacement, and Moment Release. Bulletin of the Seismological Society of America 100(5A): 1971–1988. https://doi.org/10.1785/0120090189

814 Li Q, Sun J, Xi G, Liu J (2022) The Doppler effect induced by earthquakes: A case
815 study of the Wenchuan MS8.0 earthquake. Geodesy and Geodynamics 13(5):
816 435-444. https://doi.org/10.1016/j.geog.2021.12.006

817

818 Lippiello E, de Arcangelis L, Godano C (2024) Positive Answer on the Existence
819 of Correlations between Positive Earthquake Magnitude Differences. Physical
820 Review Letters, 133(24), 244101.
821 https://doi.org/10.1103/PhysRevLett.133.244101.

822

823 Lippiello E, Godano C, de Arcangelis L (2019) The Relevance of Foreshocks in
824 Earthquake Triggering: A Statistical Study. Entropy 21(2): 1-13.
825 https://doi.org/10.3390/e21020173

826

827 Lippiello E, Petrillo G (2024) b-more-incomplete and b-more-positive: Insights on
828 a robust estimator of magnitude distribution. Journal of Geophysical Research:
829 Solid Earth, 129(2), e2023JB027849.

830

831 Colombelli S, Longobardi V, Zollo, A (2024) The deterministic behaviour of
832 earthquake rupture beginning. https://doi.org/10.21203/rs.3.rs-3967674/v1.

833

834 Martínez-Lopez MR (2023) Study of the rupture processes of the 1989 (Mw 6.9)
835 and 2021 (Mw 7.0) Guerrero earthquakes using teleseismic records:

836 Seismotectonic implications. Geologica Acta, 21(9): 1-14.
837 https://doi.org/10.1344/GeologicaActa2023.21.9

838

839 McLaskey GC, Kilgore BD (2013) Foreshocks during the nucleation of stick-slip
840 instability. Journal of Geophysical Research 118(6): 2982-2997.
841 https://doi.org/10.1002/jgrb.50232

842

843 Mogi K (1969) Some features of recent seismic activity in and near Japan (2)
844 activity before and after great earthquakes. Bulletin of the Earthquake Research
845 Institute 47(4): 395–417

846

847 Murase K (2004) A Characteristic Change in Fractal Dimension Prior to the 2003
848 Tokachi-oki Earthquake (M J = 8.0), Hokkaido, Northern Japan. Earth, Planets
849 and Space 56(3): 401–405. https://doi.org/10.1186/BF03353072

850

851 Nielsen S (2024) Earthquakes big and small: same physics, different boundary
852 conditions. arXiv preprint arXiv:2411.00544.
853 https://doi.org/10.48550/arXiv.2411.00544

854

855 Noda A, Saito T, Fukuyama E, Urata Y (2021) Energy-Based Scenarios for Great
856 Thrust-Type Earthquakes in the Nankai Trough Subduction Zone, Southwest

857 Japan, Using an Interseismic Slip-Deficit Model. Journal of Geophysical
858 Research 126(5):1-20. https://doi.org/10.1029/2020JB020417

859

860 Otarola C, Ruiz S, Herrera C, Madariaga R, Siegel C (2021) Dynamic rupture of
861 subduction earthquakes located near the trench. Earth and Planetary Science
862 Letters 562(1): 1-12. https://doi.org/10.1016/j.epsl.2021.116842

863

864 Padilla AMR, Oskin ME, Brodsky EE, Dascher-Cousineau K, Herrera V, White S
865 (2024) The Influence of Fault Geometrical Complexity on Surface Rupture
866 Length. Journal of Geophysical Research 51(20): 1-10.
867 https://doi.org/10.1029/2024GL109957

868

869 Perinelli A, Ricci L, De Santis A, Iuppa R (2024) Earthquakes unveil the global-
870 scale fractality of the lithosphere. Communications Earth & Environment 5(146):
871 1-13. https://doi.org/10.1038/s43247-023-01174-w

872

873 Pétrélis F, Chanard K, Schubnel A, Hatano T (2021) Earthquake sensitivity to
874 tides and seasons: Theoretical studies. Journal of Statistical Mechanics: Theory
875 and Experiment, 2021(2), 023404.

876

877 Posadas A, Morales J, Ibañez JM, Posadas-Garzon A (2021) Shaking earth: Non-
878 linear seismic processes and the second law of thermodynamics: A case study

879 from Canterbury (New Zealand) earthquakes. Chaos, Solitons & Fractals 151(1):
880 1-12. https://doi.org/10.1016/j.chaos.2021.111243

881

882 Renou J, Vallée M, Aochi H (2022) Deciphering the Origins of Transient Seismic
883 Moment Accelerations by Realistic Dynamic Rupture Simulations. Bulletin of the
884 Seismological Society of America 112(3): 1240-1251.
885 https://doi.org/10.1785/0120210221

886

887 Rivière J, Lv Z, Johnson PA, Marone C (2018) Evolution of b-value during the
888 seismic cycle: Insights from laboratory experiments on simulated faults. Earth and
889 Planetary Science Letters 482(1): 407-413.
890 https://doi.org/10.1016/j.epsl.2017.11.036

891

892 Rubinstein JL, La Rocca M, Vidale JE, Creager KC, Wech AG (2008) Tidal
893 modulation of nonvolcanic tremor. Science, 319(5860), 186-189.

894

895 Ruelle D (1983) Chaotic Evolution and Strange Attractors; Cambridge University:
896 New York, NY, USA, 1983

897

898 Salditch L, Stein S, Neely J, Spencer BD, Brooks EM, Agnon A, Liu M (2020)
899 Earthquake supercycles and long-term fault memory. Tectonophysics, 774,
900 228289.

Scholz CH (1990) Earthquakes as chaos. Nature 348(1): 197–198. https://doi.org/10.1038/348197a0

Scholz CH (2015) On the stress dependence of the earthquake b value. Geophysical Research Letters 42(5) 1399-1402. https://doi.org/10.1002/2014GL062863

Schurr B, Moreno M, Tréhu AM, Bedford J, Kummerow J, Li S, Oncken O (2020) Forming a Mogi Doughnut in the Years Prior to and Immediately Before the 2014 M8.1 Iquique, Northern Chile, Earthquake. Geophysical Research Letters 47(16): 1-10. https://doi.org/10.1029/2020GL088351

Sharon M, Kurzon I, Wetzler N, Sagy A, Marco S, Ben-Avraham Z (2022) Variations of the seismic b-value along the Dead Sea transform. Frontiers in Earth Science 10(1): 1-19. https://doi.org/10.3389/feart.2022.1074729

Silverio-Murillo A, Balmori-de-la-Miyar J, Sobrino F, Prudencio D (2024) Do earthquakes increase or decrease crime? World Development 182(1): 1-8. https://doi.org/10.1016/j.worlddev.2024.106711

Somerville P, Irikura K, Graves R, Sawada S, Wald D, Abrahamson N, Iwasaki Y, Kagawa T, Smith N, Kowada A (1999) Characterizing crustal earthquake slip models for the prediction of strong ground motion. Seismological Research Letters 70(1): 59–80. https://doi.org/10.1785/gssrl.70.1.59

Tabor M (1989) Chaos and Integrability in Nonlinear Dynamics; Wiley: New York, NY, USA, 1989

van der Elst NJ (2021) B-positive: A robust estimator of aftershock magnitude distribution in transiently incomplete catalogs. Journal of Geophysical Research: Solid Earth, 126(2), e2020JB021027.

Vassiliou MS, Kanamori H (1982) The energy release in earthquakes. Bulletin of the Seismological Society of America 72(2): 371–387. https://doi.org/10.1785/BSSA0720020371

Venegas-Aravena P, Cordaro E, Laroze D (2022) Fractal Clustering as Spatial Variability of Magnetic Anomalies Measurements for Impending Earthquakes and the Thermodynamic Fractal Dimension. Fractal and Fractional 6(11):1-13. https://doi.org/10.3390/fractalfract6110624

Venegas-Aravena P (2023) Geological earthquake simulations generated by kinematic heterogeneous energy-based method: Self-arrested ruptures and asperity criterion. Open Geosciences 15(1):1-20. https://doi.org/10.1515/geo-2022-0522

Venegas-Aravena P, Cordaro E (2023a) Subduction as a Smoothing Machine: How Multiscale Dissipation Relates Precursor Signals to Fault Geometry. Geosciences 13(8):1-16. https://doi.org/10.3390/geosciences13080243

Venegas-Aravena P, Cordaro E (2023b) Analytical Relation between b-Value and Electromagnetic Signals in Pre-Macroscopic Failure of Rocks: Insights into the Microdynamics' Physics Prior to Earthquakes. Geosciences 13(6), 169:1-14. https://doi.org/10.3390/geosciences13060169

Venegas-Aravena P (2024) Heterogeneous self-arrested ruptures leading to spatial variability of radiated energy and Doppler effect of the observed corner frequency. Journal of Seismology 28(1): 187–208. https://doi.org/10.1007/s10950-023-10183-3

Venegas-Aravena P, Cordaro E (2024) The Multiscale Principle in Nature (Principium luxuriæ): Linking Multiscale Thermodynamics to Living and Non-Living Complex Systems. Fractal and Fractional 8(1):1-43. https://doi.org/10.3390/fractalfract8010035

966

967 Venegas-Aravena P, Crempien JGF, Archuleta RJ (2024) Fractal Spatial
968 Distributions of Initial Shear Stress and Frictional Properties on Faults and Their
969 Impact on Dynamic Earthquake Rupture. Bulletin of the Seismological Society of
970 America 114(3): 1444–1465. https://doi.org/10.1785/0120230123

971

972 Vidale JE, Agnew DC, Johnston MJ, Oppenheimer DH (1998) Absence of
973 earthquake correlation with Earth tides: An indication of high preseismic fault
974 stress rate. Journal of Geophysical Research: Solid Earth, 103(B10), 24567-
975 24572.

976

977 Vieira MdS (1999) Chaos and Synchronized Chaos in an Earthquake Model.
978 Physical Review Letters 82(1): 201-204.
979 https://doi.org/10.1103/PhysRevLett.82.201

980

981 Wallace LM, Fagereng Å, Ellis S (2012) Upper plate tectonic stress state may
982 influence interseismic coupling on subduction megathrusts. Geology 40(10):
983 895–898. https://doi.org/10.1130/G33373.1

984

985 Wang Z, Zhang W, Taymaz T, He Z, Xu T, Zhang Z (2023) Dynamic Rupture
986 Process of the 2023 Mw 7.8 Kahramanmaraş Earthquake (SE Türkiye): Variable
987 Rupture Speed and Implications for Seismic Hazard. Geophysical Research
988 Letters 50(15):1-11. https://doi.org/10.1029/2023GL104787

989

990 Wetzler N, Lay L, Brodsky EE (2023) Global Characteristics of Observable
991 Foreshocks for Large Earthquakes. Seismological Research Letters 94(5): 2313–
992 2325. https://doi.org/10.1785/0220220397

993

994 Woessner J, Wiemer S (2005) Assessing the quality of earthquake catalogues:
995 Estimating the magnitude of completeness and its uncertainty. Bulletin of the
996 Seismological Society of America, 95(2), 684-698.

997

998 Wyss M (1997) Cannot Earthquakes Be Predicted? Science 278(5337): 487-490.
999 https://doi.org/10.1126/science.278.5337.487

1000

1001 Wyss M, Sammis CG, Nadeau RM, Wiemer S (2004) Fractal Dimension and b-
1002 Value on Creeping and Locked Patches of the San Andreas Fault near Parkfield,
1003 California. Bulletin of the Seismological Society of America 94 (2): 410–421.
1004 https://doi.org/10.1785/0120030054

1005

1006 Xie H (1993) Fractals in Rock Mechanics, 1st ed.; CRC Press: Boca Raton, FL,
1007 USA

1008

Yılmaz N, Akıllı M, Ak M (2023) Temporal evolution of entropy and chaos in low amplitude seismic wave prior to an earthquake. Chaos, Solitons & Fractals 173(1): 1-11. https://doi.org/10.1016/j.chaos.2023.113585

Zaccagnino D, Vallianatos F, Michas G, Telesca L, Doglioni C (2024) Are Foreshocks Fore-Shocks? Journal of Geophysical Research 129(2): 1-17. https://doi.org/10.1029/2023JB027337

Zou X, Fialko Y (2024) Can Large Strains Be Accommodated by Small Faults: “Brittle Flow of Rocks” Revised. Earth and Planet Science 11(11): 1-16. https://doi.org/10.1029/2024EA003824